Edith Cowan University

Research Online

1-1-2013

Optical Magnetometer Employing Adaptive Noise Cancellation for Unshielded Magnetocardiography

Valentina Tiporlini
Edith Cowan University, v.tiporlini@ecu.edu.au

Kamal Alameh
Edith Cowan University, k.alameh@ecu.edu.au

Optical Magnetometer Employing Adaptive Noise Cancellation for Unshielded Magnetocardiography

Valentina Tiporlini[*], Kamal Alameh

Electron Science Research Institute, Edith Cowan University, Joondalup, 6027 WA, Australia
*Corresponding author: vtiporl0@our.ecu.edu.au

Abstract   This paper demonstrates the concept of an optical magnetometer for magnetocardiography. The magnetometer employs a standard Least-Mean-Squares (LMS) algorithm for heart magnetic field measurement within unshielded environment. Experimental results show that the algorithm can extract a weak heart signal from a much-stronger magnetic noise and detect the P, QRS, and T heart features and completely suppress the common power line noise component at 50 Hz.

Keywords   Magnetocardiography; Optical Magnetometry; Adaptive Noise Cancellation; Least-Mean-Squares Algorithm

1. Introduction

The human heart is made of conductive tissues that produce both an electric field and a magnetic field, depending on cardiac activity. Measuring the electric and/or magnetic fields enables various heart parameters as well as diseases to be diagnosed, such as heart beat rate and arrhythmia. In particular, fetal heart rate monitoring is crucial not only for collecting useful information on the wellbeing of a pregnancy but also for the early diagnosis of fetal distress and a prompt intervention in case of adverse events. Electrocardiography (ECG) enables the detection of heart-generated electric fields through electrodes placed on the surface of the human body, so that only the effects of currents flowing through the body tissues are detected. These currents are affected by local inhomogeneities due to discontinuities of the electric conductivity in the body tissues, such as fat layers or bones that act as spatial low-pass filters. Furthermore, ECG has disadvantages related to skin-electrode contacts, including: (i) measurement dependence upon the position of the electrodes, (ii) addition of electrode-contact noise due to loss of adherence between the electrode and the skin, (iii) motion artifacts caused by the skin and electrode interface and electrode cable and (iv) unsuitability for patients with damaged skin, such as acute burns. Techniques based on magnetic fields measurements offer a simple non-invasive method for the collection of electrophysiological waveforms without any physical contact between the device and the patient, and hence, problems arising from skin-electrode contact are avoided. Furthermore, magnetocardiography (MCG) has been shown to be more accurate than electrocardiography for the (i) diagnosis of atrial and ventricular hypertrophy, (ii) non-invasive location of the heart's conduction pathways, (iii) the identification of spatial current dispersion patterns, and (iv) the detection of circular vortex currents which give no ECG signal [1]. Cardiac magnetic fields surround the human body and are typically very low in magnitude (about 100 pT for adults [2] and between 5 to 10 pT for a fetus [3]). Therefore, the measurement of a very weak heart-generated magnetic field requires high sensitivity magnetometers. Furthermore, the environmental electromagnetic noise is typically much stronger than the cardiac magnetic field necessitating the magnetocardiographic measurements to be run inside a magnetically-shielded room, thus making conventional magnetometers expensive and impractical for dynamic hospital environments.

Typically superconducting quantum interference devices (SQUID) that have a demonstrate sensitivity of the order of $fT/\sqrt{Hz}$ [4] are used in magnetocardiography. Optical magnetometers that use the magnetically dependent optical property of certain media have demonstrated sensitivities as high as those of SQUID based magnetometers and start to be vastly used in magnetocardiography [5]. Moreover, SQUID based magnetometers must be operated at very low temperatures, thus requiring cumbersome and expensive cooling mechanisms. Optical magnetometers have the advantage of working at room temperature and also have the potential of miniaturization (they can be fitted in a volume of $1mm^3$ [6, 7]), making them more practical for many applications. The main problem of magnetocardiography is the environmental electromagnetic noise, generated by the power supply and electronic devices, that is typically much higher (in the order of nT) than the heart-generated magnetic field. This results in an extremely low signal-to-noise ratio, if patients are examined outside a magnetic shielded room.
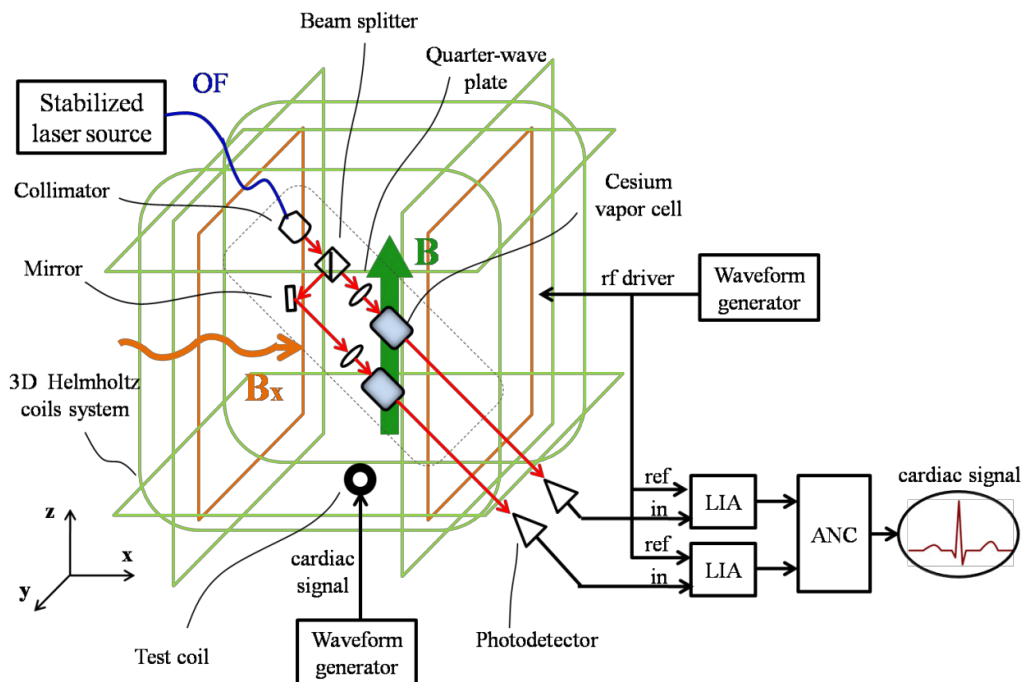
Figure 1. Experiment setup that demonstrates the principle of the proposed optical magnetometer.

The aim of operating the magnetocardiographic system in magnetically noisy environments creates the need for developing effective noise suppressing techniques. Magnetic noise suppression in magnetically unshielded environments has been demonstrated based on the use of an array of magnetometers. For example, the performance of a multichannel system based on SQUID magnetometry in an unshielded environment has been shown to be comparable with magnetic field measurements performed inside a shielded room [8]. The application of an efficient noise cancellation system based on adaptive signal processing has been used to improve the measurement of SQUID based magnetocardiographic signals in an unshielded environment [9].

In this paper, we propose and demonstrate the concept of an optically-pumped quantum magnetometer capable of measuring a cardiac magnetic signal in unshielded environment. We particularly adopt a standard adaptive Least-Mean-Squares (LMS) algorithm, which has commonly been used in electrocardiography for removing low spectral noise components [10, 11]. The paper is organized as follows: in Section II, the optically-pumped quantum magnetometer and the adaptive noise cancellation system used for heart beat sensing are described; in Section III experimental results are reported and discussed and concluding remarks are presented in Section IV.

2. Optical Magnetometer

Conventional optically-pumped quantum magnetometers are based on the use of the atomic-spin-dependent optical properties of a medium. The principle of operation of optically-pumped quantum magnetometers is described in detail in [12]. A circularly polarized laser light transmitted through a glass cell containing a vapor of alkali atoms (e.g., Cesium) resonates when its frequency equals to the first absorption line of the alkali atoms. This creates a spin alignment that precesses with a frequency proportional to the modulus of an externally applied magnetic field, B_0. This precession frequency is called Larmor frequency and is defined as: $w_L = \gamma |B_0|$, where γ is the gyromagnetic constant, which has a value of $2\pi \times 3.5$ Hz/nT for Cesium. If this precession is coherently driven by a radiofrequency (rf) magnetic field, B_{rf} (oscillating at frequency w_{rf}), the absorption coefficient of the alkali medium changes, thus modulating the transmitted optical intensity. Such magnetometers are known as Mx magnetometers because the rf oscillating magnetic field supplied to the vapor atoms modulates the x component of the magnetization vector inside the vapor cell [13]. The phase difference between the driving rf signal and the probe light transmitted through the vapor cell gives a direct measurement of the Larmor frequency.

We adopt the Mx magnetometer configuration shown in Figure 1, through an experimental setup, which is similar to that described in [14] with one key difference, which is the addition of one cell that senses the environmental noise. A 3-D electromagnet system was used to generate a dc magnetic field that cancels the geomagnetic field and supplies a uniform magnetic field thus producing appropriate magnetization vector along the z-direction inside the two vapor cells. The used electromagnet consisted of two parts: (i) a 3-D DC coils of dimension 580mm×530mm×640mm providing a magnetic field with a uniformity better than 1% in the central region; and (ii) an additional pair of coils that

generate a small-magnitude rf magnetic field along the x axis. Each coil-pair of the electromagnet was independently driven by a digital power supply to cancel the geomagnetic field along the x and y directions, and generate a uniform magnetic field along the z-axis. The intensity of the magnetic field at the center of the electromagnet was 8μT, as measured by a Honeywell HMR2300 three-axes smart digital magnetometer. The AC coils were driven by a waveform generator to produce an rf magnetic field of intensity of 200nT, oscillating at a frequency of 28 kHz along the x-axis. Two vapor cells, which constituted the core of the instrument, were placed in the center of the electromagnet and used to implement a noise cancellation system, since it required two sensors to measure the heart magnetic field and the environmental noise. In addition to Cesium vapor, Neon at 34Torr and Argon at 6Torr were added to the cells in order to reduce atom collisions. The cells diameter and length were 21mm and 75mm, respectively, yielding a spatial resolution of about 53mm, when tilted by 45° with respect to the z-axis. The distance between the cells was made 10cm to assure that the reference cell is not affected by the cardiac signal. In the experiments, the gas pressure inside the cells was increased by increasing the cells temperature through hot water flowing into a silicon pipe wrapped around the cells. The temperature of the vapor cells was increased to 37°C, which corresponds to the typical human body temperature. An external-cavity semiconductor laser was used as the light source for both pumping and probing. The laser wavelength was tuned to 894nm which corresponds to the Cesium D1 absorption line F=4→F=3 transition, and stabilized using saturation spectroscopy in an auxiliary cell. The frequency-stabilized light was coupled into a single-mode polarization maintaining optical fiber of 5μm core diameter, collimated at 1.6mm diameter, split to two laser beams using a polarization beam splitter (PBS). The two laser beams are then circularly polarized using two quarter-wave plates, and then transmitted through the vapor cells inside the electromagnet. The power of each laser beam before transmission through the corresponding vapor cell was 20μW. After emergence from the vapor cells, the output laser beams were focused and detected by two optical receivers, which were placed outside the electromagnet in order to reduce the magnetic interference produced by the transimpedance amplifier of each photodiode package. Finally, the phase shifts between the photocurrents detected by the photodiodes with respect to the oscillating rf magnetic field were measured using a lock-in amplifier. These measured phase shift signals were used as the input noisy signal and noise reference for an adaptive noise cancellation system based on standard LMS algorithm.

Adaptive noise suppression techniques are typically based on adaptive filtering and require very little or no prior knowledge of the signal of interest. To suppress the noise, a reference input signal is required, which is typically derived from one or more magnetic sensors placed at positions where the noise level is higher than the signal amplitude. Figure 2 shows a block diagram of an adaptive noise canceller applied to a generic magnetic heart field measurement. The primary

input to the canceller, denoted d(k), is the sum of the signal of interest s(k) and the noise n(k), which is typically uncorrelated with s(k). The reference input signal of the system, x(k), is a noise that is correlated in some unknown way with n(k), but uncorrelated with the signal of interest s(k).
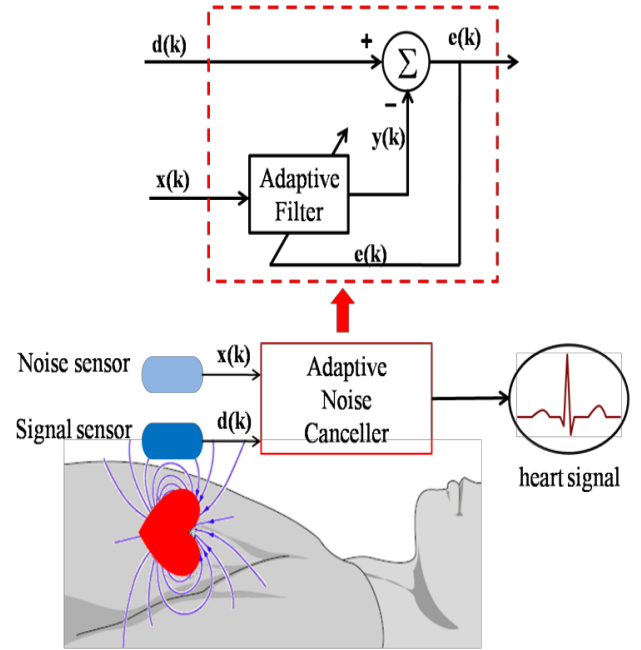

Figure 2. Typical block diagram of an adaptive noise canceller.

As shown in Figure 2, x(k) is adaptively filtered to produce a replica of the noise n(k) that can be subtracted from the primary input to eventually produce an output signal e(k) equals to s(k). The objective of the noise canceller is to minimize the mean-squared error between the primary input signal, d(k), and the output of the filter, y(k) [15].

Referring to Figure 2, the output signal is given by

$$e(k) = d(k) - y(k) = s(k) + n(k) - y(k) \quad (1)$$

Therefore, the mean-squared of e(k) is given by

$$E\{e^2(k)\} = E\{s^2(k)\} + E\{(n(k)-y(k))^2\} \\ + 2E\{s(k)(n(k)-y(k))\} \quad (2)$$

Since s(k) is uncorrelated with n(k) and y(k), the last term in (2) is zero, yielding:

$$E\{e^2(k)\} = E\{s^2(k)\} + E\{(n(k)-y(k))^2\} \quad (3)$$

It is noticed from (3) that the mean-squared error is minimum when n(k) = y(k), and hence, when the output signal e(k) is equal to the desired signal s(k).

The LMS algorithm aims to minimize the mean-squared error by calculating the gradient of the squared-error with respect to the coefficients of the filter. Assuming that the adaptive filter is a FIR filter of order M, then (1) becomes:
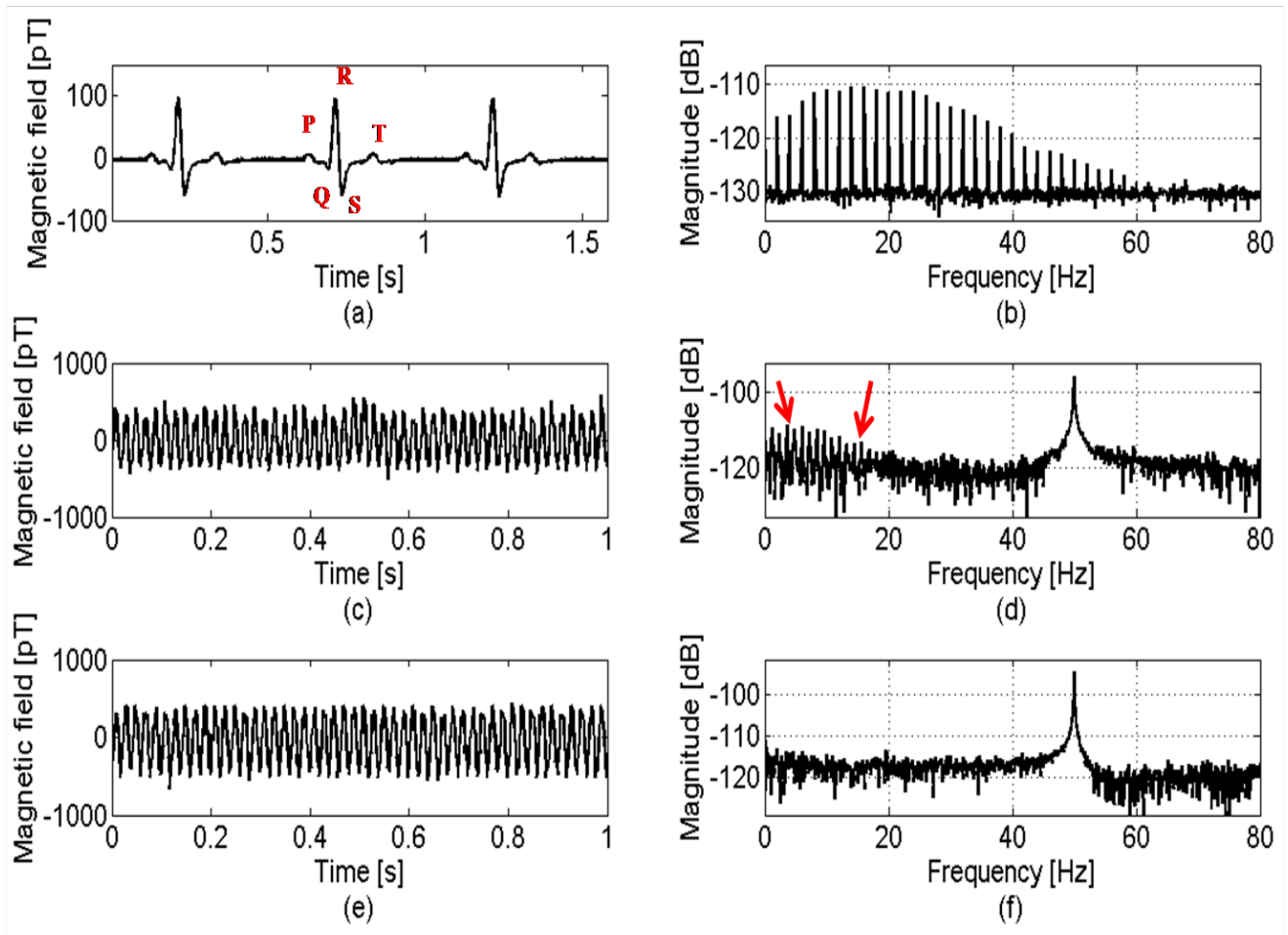
$$e(k) = d(k) - \sum_{i=0}^{M-1} b_i x(k-i) \quad (4)$$

Figure 3. a) Heart signal generated using a heart waveform generator. The typical P wave, QRS complex and T wave, are clearly displayed, which correspond to atrial depolarization, ventricular depolarization and ventricular repolarization, respectively; b) spectrum of the generated heart signal, which is mainly concentrated at low frequencies (from DC to 60Hz); c) signal measured by the sensor close to the heart; d) spectrum of the signal measured by the sensor closest to the heart (red arrows point to the low-frequency components of the heart signal); e) noise measured by the reference sensor and f) spectrum of the noise measured by the reference sensor.

The updating procedure is applied on coefficients b_i according to the following rule [16]:

$$b_i^{(k+1)} = b_i^{(k)} + 2\mu e(k)x(k-i) \qquad (5)$$

where $i = 0,1,\ldots,M-1$, k is the iteration index and μ is the step size that indicates the adaption rate of the algorithm and is usually included in the range (0,1]. The LMS algorithm can have high convergence time especially if the noise to be removed is much larger than the signal. To increase the convergence speed, a variable adaption rate can be used. This is a variant of the LMS algorithm called normalized LMS. Equation (5) now can be written [16]:

$$b_i^{(k+1)} = b_i^{(k)} + 2\mu_k e(k)x(k-i) \qquad (6)$$

where $\mu_k = \dfrac{\mu_n}{\|x(k)\|^2}$, $\qquad 0 < \mu_n < 2$

The normalization of the LMS step size by $\|x(k)\|^2$ typically reduces the convergence time.

It is important to mention that all the experimental results reported below were performed outside of a magnetically shielded room in laboratory environment, which was contaminated with a high level of electromagnetic noise. This noise is attributed to various electric equipments, such as power supplies, computers, transmitters for wireless network and mobile phones. Typically, optical Mx magnetometers operate in phase-locked mode with a feedback loop implemented between the lock-in amplifier phase output and the driver of the AC coils. Specifically, the rf frequency is locked to the cell that measures the environmental noise [17]. This approach enables the signal measured by the close-to-the-heart cell to sense the change due to the heart field only with minimum noise contamination. Our novel approach is based on operating the Mx magnetometer in a free-running mode without the use of feedback between the lock-in amplifier and the rf driver. This method assures a high-level of correlation between the noisy signal and noise reference, and makes the noise cancellation more efficient in accurately recovering the heart signal. A heart signal spectrum typically spreads over a bandwidth of at least 60 Hz.

The main problem in the proposed free-running mode configuration of the Mx magnetometer was the limited bandwidth of the magnetometer. This issue was overcome by setting the time constant of the output filter of the lock-in amplifier to 1 second. The process that was used for the extraction of the heart signal from the noise was based on (i) recording the phase shift signals from the lock-in amplifiers over a period of around 8 seconds, (ii) processing the recorded signals offline using the LMS algorithm and the normalized LMS algorithm to recover the heart signal, (iii) repeating steps (i) and (ii) for different time periods (more than 50 times), and (iv) calculating the average of the extracted signals to obtain the final heart signal.
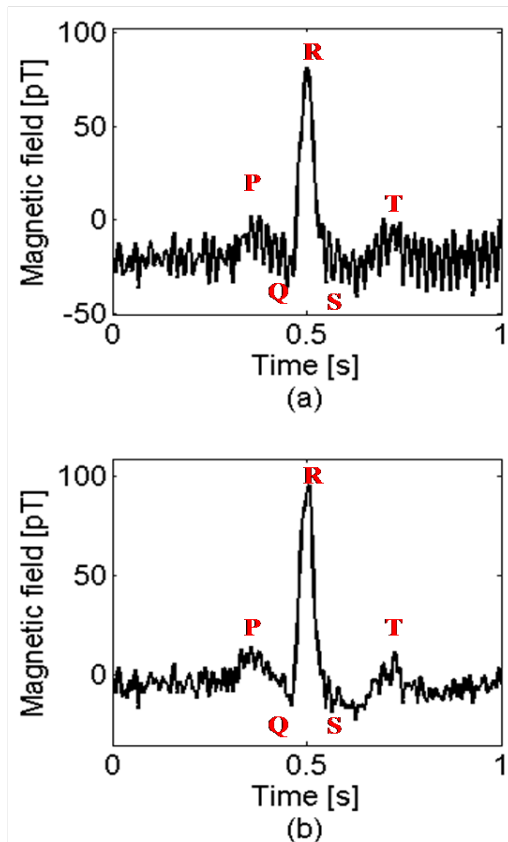

Figure 4. Magnetic heart signals extracted by (a) LMS algorithm and (b) normalized LMS algorithm.

3. Experimental Results and Discussion

A test coil was placed inside the electromagnet system to simulate the human heart activity. The distance between the test coil and the center of the vapor cell was 5cm. A waveform generator was used to produce a cardiac signal and drive the test coil. The frequency of the generated cardiac test field was 1.2 Hz, which corresponds to the typical human heart rate of 70 beats per minute. Figure 3 (a) shows the waveform of the generated heart signal where the typical cardiac features are clearly displayed, namely, P wave, QRS complex and T wave, which correspond to atrial depolarization, ventricular

depolarization and ventricular repolarization, respectively. Figure 3 (b) shows the spectrum of the cardiac signal that typically spreads over low frequencies, exactly between DC to 60Hz. Figures 3 (c and d) show the waveform and the corresponding spectrum of the signal detected by the sensor that was close to the heart, named Signal Sensor in Figure 2. Figures 3 (e and f) display the waveform and the corresponding spectrum of the reference noise detected by the other sensor, named Noise Sensor in Figure 2. The waveforms shown in Figures 3 (c and e) are the main input signals needed to recover the heart signal by the noise cancellation algorithm. From Figure 3 (c) is obvious that the noise is much stronger than the heart signal, making the heart beat unremarkable. As shown from Figures 3 (d and f), the main source of noise in the frequency range of interest is the interference at 50 Hz produced by power lines. However, the low-frequency components of the heart signal are clearly seen in Figure 3 (d) (pointed to by the red arrows). Since the heart signal is concentrated in the DC-60Hz range, both inputs of the noise canceller were filtered using a low pass filter with a cutoff frequency of 90 Hz.
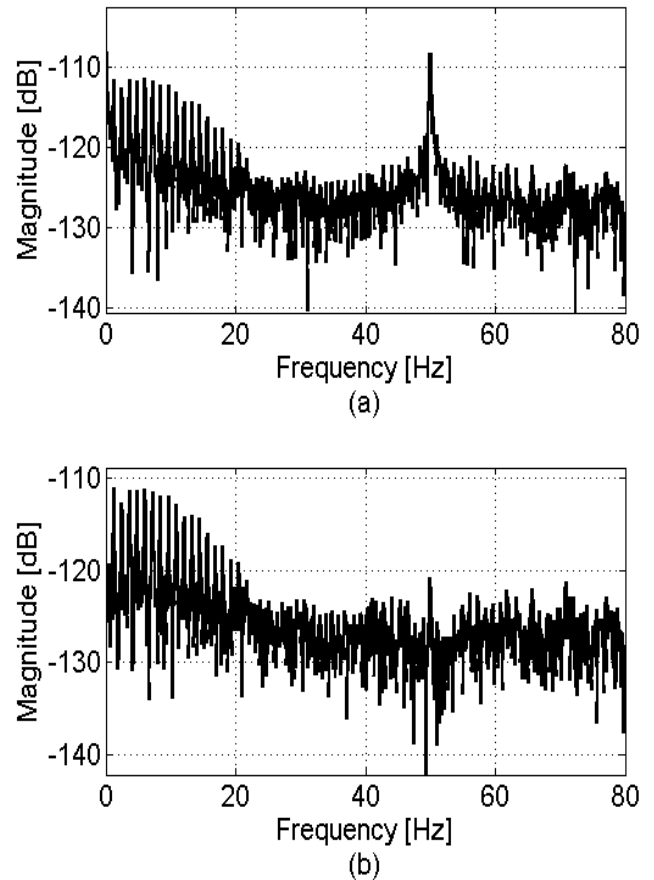

Figure 5. Spectrum of the heart signal extracted by (a) LMS algorithm and (b) normalized LMS algorithm.

Figures 4 (a and b) show the cardiac signal extracted from the signals displayed in Figures 3 (c and e) using the adaptive noise canceller based, respectively, on (i) LMS algorithm and (ii) normalized LMS algorithm. It is important to note that the

results shown in Figure 4 were averaged over 50 measurements. Both the LMS algorithm and the normalized LMS algorithm were capable of clearly detecting the QRS complex, enabling the prediction of the heart rate. Note that the P and T waves were better identified with the normalized LMS algorithm. Figures 5 (a and b) show the spectra of the heart signals recovered by the LMS algorithm and the normalized LMS algorithm, respectively. It is obvious that while both algorithms successfully recovered the heart waveform, the normalized LMS algorithm outperformed the LMS algorithm in canceling the noise component at 50Hz.

The experimental demonstrator successfully recovered a heart signal (simulated with a test coil) as well as all its typical features in an unshielded environment, with the recovered signal being comparable to those recovered by ECG and MCG systems working inside a shielded room.

4. Conclusion

An Mx-configuration-based optically-pumped quantum magnetometer employing two sensing cells in conjunction with a standard LMS-algorithm-based adaptive noise canceller has been developed, and its capability of measuring heart generated magnetic fields has been experimentally demonstrated in magnetically-unshielded environment. The use of LMS and normalized LMS algorithms has been investigated for suppressing the power line generated 50Hz interference and recovering of heart waveforms. Both algorithms have successfully detected the P, QRS, and T heart features. However, the normalized LMS algorithm has outperformed the LMS algorithm in the cancellation of 50Hz noise component. The results shown in this paper are useful for signal processing in magnetocardiographic system operating in unshielded environment.

REFERENCES

[1] F. E. Smith, et al., "Comparison of magnetocardiography and electrocardiography: a study of automatic measurement of dispersion of ventricular repolarization," The European Society of Cardiology, vol. 8, pp. 887-893, 2006.

[2] G. Bison, R. Wynards, and A. Weis, "Dynamical mapping of the human cardiomagnetic field with a room-temperature, laser-optical sensor," Optics Express, vol. 11, pp. 904-909, 2003.

[3] J. Q. Campbell, et al., "Fetal Magnetocardiographic Source Separation: Independent Component Analysis Techniques and Signal-Space Projection," International Journal of Bioelectromagnetism, vol. 7, pp. 329-333, 2005.

[4] "Superconducting Quantum Interference Device: the most sensitive detector of magnetic flux," Tamkang Journal of Science and Engineering, vol. 6, pp. 9-18, 2003.

[5] G. Bison, R. Wynands, and A. Weis, "A laser-pumped magnetometer for the mapping of human cardiomagnetic fields," Applied Physics B-Lasers and Optics, vol. 76, pp. 325-328, Mar 2003.

[6] V. Shah, S. Knappe, P. D. D. Schwindt, and J. Kitching, "Subpicotesla atomic magnetometry with a microfabricated vapour cell," Nature Photonics, vol. 1, pp. 649-652, Nov 2007.

[7] L. A. Liew, et al., "Microfabricated alkali atom vapor cells," Applied Physics Letters, vol. 84, pp. 2694-2696, Apr 5 2004.

[8] R. Fenici, D. Brisinda, A. M. Meloni, and P. Fenici, "First 36-Channel System for Clinical Magnetocardiography in Unshielded Hospital laboratory for Cardiac Electrophysiology," International Journal of Bioelectromagnetism, vol. 5, pp. 80-83, 2003.

[9] M. Bick, et al., "SQUID gradiometry for magnetocardiography using different noise cancellation techniques," IEEE Transactions on Applied Superconductivity, vol. 11, pp. 673-676, 2001.

[10] N. V. Thakor and Z. Yi-Sheng, "Applications of adaptive filtering to ECG analysis: noise cancellation and arrhythmia detection," IEEE Transactions on Biomedical Engineering, vol. 38, pp. 785-794, 1991.

[11] M. Rahman, R. Shaik, and D. V. R. Reddy, "Cancellation of Artifacts in ECG Signals Using Block Adaptive Filtering Techniques," in Software Tools and Algorithms for Biological Systems. vol. 696, H. R. Arabnia and Q.-N. Tran, Eds., ed: Springer New York, 2011, pp. 505-513.

[12] D. Budker and M. Romalis, "Optical magnetometry," Nat Phys, vol. 3, pp. 227-234, 2007.

[13] G. Bison, R. Wynands, and A. Weis, "Optimization and performance of an optical cardiomagnetometer," Journal of the Optical Society of America B-Optical Physics, vol. 22, pp. 77-87, Jan 2005.

[14] V. Tiporlini and K. Alameh, "High Sensitivity Optically Pumped Quantum Magnetometer," The Scientific World Journal, vol. 2013, p. 8, 2013.

[15] B. Widrow, et al., "Adaptive Noise Cancelling: Principles and Applications," Proceedings of the IEEE, vol. 63, pp. 1692-1716, 1975.

[16] P. S. R. Diniz, "Adaptive Filtering Algorithms and Practical Implementation," Springer, 2008.

[17] "Atomic Vector Gradiometer System Using Caesium Vapour cells for magnetocardiography: Perspective on Practical Application," IEEE Transactions on Instrumentation and Measurement, vol. 56, pp. 458-462, 2007.